CHAPTER 3

Diffuse dust emission in the Large Magellanic Cloud

The diffuse emission from several locations in the Large Magellanic Cloud (LMC) has been observed by the *Far Ultraviolet Spectroscopic Explorer (FUSE)* space telescope with intensities ranging from 1000 to 3×10^5 photon units and diffuse fraction between 5% and 20% at 1100 Å. The intensity ratios in different far-ultraviolet (FUV) and infrared (IR) bands enable us to determine the type of dust contributing to the diffuse emission at these locations as well as to derive a more accurate 3D distribution of stars and dust in the region; which in turn may be used to model the observed dust scattering in the FUV. The emission/scattering depends not only on the amount of dust present, but also on the rate of heating by starlight. In this chapter, we present the IR data for two HII regions in LMC, namely N11 and 30 Doradus along with the FUV-IR correlations at the observed diffuse dust locations.

3.1 Introduction and Motivation

The Magellanic Clouds are the nearest systems which offer an opportunity for the study of extragalactic abundances [119]. Four types of objects are available for studies of this sort: normal stars, supernova remnants, planetary nebulae, and HII regions. The Large Magellanic Cloud (LMC) provides a nearby, ideal laboratory to study the influence of massive stars on dust properties because it has a nearly face-on orientation, mitigating the confusion and extinction along the Galactic plane. It is at a known distance, ∼50 kpc [120] and hence the stars can be resolved and studied in conjunction with interstellar gas and dust [121]. The LMC is located at a high latitude ($\sim 30^0$) [122] and therefore it is not much affected by extinction from the Milky Way (MW) dust. For these reasons, the LMC has been targeted by every space-based IR observatory to study dust properties and calibrate dust emission as star formation indicators. The highest reddening in the LMC occurs in the 30 Doradus and supershell LMC 2 regions with a maximum color excess, E(B-V)≈0.29. The N11 region also shows high reddening effects with E(B-V)≈0.24 [123].

The first report of *Spitzer Space Telescope* observations of an LMC HII complex was made by Gorjian et al. (2004)[124] for LHA120-N206 (N206) [125], who qualitatively compared its dust emission to that in the Orion nebula. Subsequently, the entire LMC was surveyed by *Spitzer* in the Legacy program Surveying the Agents of a Galaxy's Evolution (SAGE) [126]. The Very Small Grain (VSG) emission detected in the *Spitzer* 24 μm band [104] is seen to be associated with locations close to hot UV emitting stars such as HII regions, just like the dust scattered UV radiation. However, the behaviour of Polycyclic Aromatic Hydrocarbon (PAH) emission in cluster environments has not been studied well [127] mainly due to sparse filter sampling in the 8-24 μm range of *Spitzer* [128]. In contrast, the Japanese *AKARI* satellite [129] has continuous wavelength coverage in the 2-24 μm range with nine photometric bands observed by the *AKARI* Infrared Camera (IRC) [78].

Therefore, by studying the locations which show diffuse emission in the FUV and IR, we hope to identify the particular grain population responsible for the observed emissions. We expect to find a better correlation between the FUV and 24 μm intensities near hot O and B-type stars as compared to the FUV vs. 8 μm correlation.

3.2 Sample of Observations

We have selected a list of 81 diffuse locations observed in the LMC by Pradhan et al. (2010) [130] using *FUSE* observations. The *FUSE* spacecraft included three apertures: the HIRS ($1.25'' \times 20''$), the MDRS ($4'' \times 20''$) and the LWRS ($30'' \times 30''$), all of which obtained data simultaneously. Only the LWRS, with its relatively large field of view, was useful for diffuse observations. Murthy & Sahnow (2004) [110] have described the analysis of the background observations and Pradhan et al. (2010) [130] have followed their method of extraction of diffuse surface brightness from the *FUSE* spectra. The *FUSE* spectrum is treated as a broadband photometric observation and the spectra was collapsed into two wavelength bands per detector, excluding the terrestrial airglow lines (primarily Lyβ). This results in seven wavelength bands with effective wavelengths at 1004 Å (1A1), 1058 Å (1A2), 1117 Å (1B1), 1157 Å (1B2), 1159 Å (2A1), 1112 Å (2A2) and 1056 Å (2B1) [130].

Among the 81 locations observed by *FUSE*, 43 were available in the *Spitzer* and *AKARI* archives and have been considered for this work. The *Spitzer* archive had 15 locations observed by the Infrared Array Camera (IRAC) at 8 μm and by the Multiband Imaging Photometer for Spitzer (MIPS) at 24

μm. The *AKARI* archive had 28 locations with 15 μm and 24 μm observations which were taken by the Infrared Camera (IRC) using the MIR-L system (12.4-26.5 μm). The 24 μm band of *Spitzer* (128 $\times$ 128 pixels) has a different resolution as compared to the *AKARI* (256 $\times$ 256 pixels) 24 μm and the concerned locations are different as we did not find any location with overlapping *Spitzer* and *AKARI* 24 μm data. One of the advantages of *AKARI* IRC was the large size of detector arrays which enabled it to observe 10 square arcmins at a time. We have also used 28 locations observed by the *AKARI* Far-Infrared Surveyor (FIS) using the WIDE-S band centered at 90 μm which made all-sky surveys in the far-IR. The instrument details of IRAC, MIPS, IRC, and FIS have been discussed in Section 1.2.1.

Our locations were generally around well-studied targets in the LMC such as the 30 Doradus (Tarantula Nebula) and the N11 which are HII regions in the LMC; as shown in Figure 3.1.

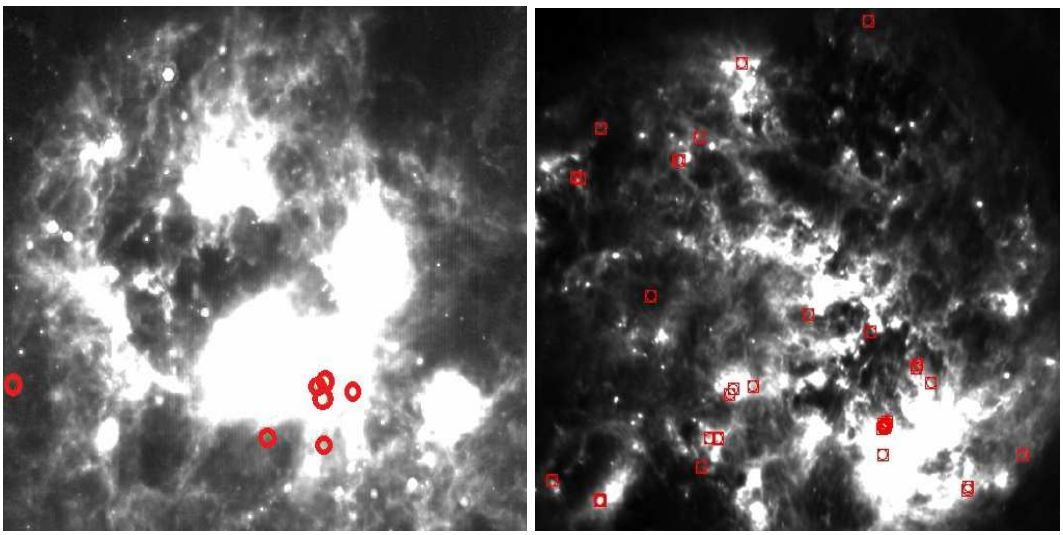

Figure 3.1: LMC images taken by the *Spitzer Space Telescope* at 8 μm (left) showing the N11 and the *AKARI* satellite at 24 μm (right) showing the 30 Doradus in the mid-IR with our locations represented in red circles and squares.

3.3 Data analysis and Results

We have used aperture photometry technique discussed in Section 1.3.1 in order to determine the intensity values for all the 43 diffuse locations and the results are presented in Table 3.1 for the 15 locations observed by *Spitzer* and Table 3.2 for the 28 locations observed by *AKARI*. The aperture size while calculating the intensity values has been taken as $30'' \times 30''$ which is the same as the aperture size of *FUSE* LWRS which has been used to obtain the FUV

intensities [130]. The coordinates used are galactic longitude (gl) and galactic latitude (gb). I_8 refers to intensity at 8 μm wavelength; similarly for I_{15}, I_{24} and I_{90}. The intensities (I_8, I_{15}, I_{24}, I_{90}) are in units of MJy sr^{-1}. The Henize numbers for the locations have been taken from the catalogue by Henize (1956) [125]. The other details have been taken from astronomical databases NED and SIMBAD.

Table 3.1: Details of the 15 locations observed by *Spitzer* in the LMC.

gl	gb	I_8 (MJy sr^{-1})	I_{24} (MJy sr^{-1})	Henize No./Comments
280.9115	-35.8492	0.90 ± 0.18	21.69 ± 0.48	N77A, N77D (HII region)
282.6024	-35.2981	0.21 ± 0.12	20.61 ± 0.09	N78 (Emission nebula)
278.8562	-36.3031	1.49 ± 0.11	20.51 ± 0.07	N3 (Exciting star)
278.2105	-36.0629	0.98 ± 0.21	21.07 ± 0.18	S3 (C1 object in NGC 1735)
277.2729	-36.2522	0.69 ± 0.19	16.89 ± 0.13	S2 (Emission-line star)
278.2475	-36.0221	1.29 ± 1.03	16.36 ± 0.11	S3 (C1 object in NGC 1735)
279.8756	-35.5509	2.19 ± 0.16	16.03 ± 0.05	N84 (Emission nebula)
277.1267	-36.0851	2.23 ± 0.21	17.76 ± 0.23	N11, N11B (HII region, HD 32256)
277.1008	-36.0451	4.38 ± 1.08	19.16 ± 0.36	N11A (HII region, HD 32340)
279.4643	-35.5125	0.70 ± 0.20	21.04 ± 0.42	N91 (HII region, NGC 1770)
277.1354	-36.0335	6.98 ± 2.61	26.97 ± 3.30	N11A (HII region, HD 32340)
277.1473	-36.0309	20.78 ± 7.73	60.05 ± 39.05	N11A (HII region, HD 32340)
277.1460	-36.0271	30.87 ± 24.11	83.59 ± 52.14	N11A (HII region, HD 32340)
279.4828	-35.4927	2.32 ± 0.32	20.26 ± 0.39	N91 (HII region, NGC 1770)
277.1277	-36.0103	7.14 ± 1.30	23.45 ± 1.63	N11A (HII region, HD 32340)

Once we obtained the IR intensities of the diffuse dust locations corresponding to those observed in the FUV by Pradhan et al. (2010) [130], we calculated the Spearman's rank correlations among the intensity values at 8 μm, 15 μm, 24 μm and 90 μm separately with all seven *FUSE* wavelength bands in the FUV. The Spearman's rank correlation and the importance of p-value have been discussed in Section 1.3.2.

We observe that there is no significant change in correlation trend when we consider all seven FUV wavelength bands from 1004-1159 Å. Hence, we have presented the rank correlation values and corresponding plots for only the first case, i.e. IR vs. FUV 1A1 (1004 Å). The correlation coefficients for *Spitzer* IR data at 8 μm and 24 μm vs. *FUSE* FUV 1A1 are shown in Table 3.3. The corresponding plots are shown in Figure 3.2. The rank correlations for *AKARI* IR data at 15 μm, 24 μm and 90 μm vs. *FUSE* FUV 1A1 are shown in Table 3.4 with the corresponding plots shown in Figure 3.4. We have also calculated the correlations separately for the dust locations in the N11 and 30 Doradus HII regions of the LMC, which have been shown with brackets (N11, 30D) in Tables 3.3 and 3.4. The N11 and 30D plots are shown in Figures 3.3 and 3.5.

Table 3.2: Details of the 28 locations observed by *AKARI* in the LMC.

gl	gb	I_{15} (MJy sr^{-1})	I_{24} (MJy sr^{-1})	I_{90} (MJy sr^{-1})	Henize No./Comments
278.1417	-34.5918	5.84 ± 2.48	9.64 ± 5.36	6.86 ± 0.06	N25 (Emission nebula)
279.7050	-33.3704	17.72 ± 8.34	78.61 ± 19.20	19.02 ± 0.43	S99, N120 (SNR, NGC 1918)
275.7129	-33.7330	46.34 ± 12.87	65.15 ± 23.61	24.85 ± 2.40	N40, N43 (NGC 1923)
278.3468	-33.2801	97.19 ± 47.31	249.71 ± 79.21	153.25 ± 20.52	N44 (HD 269404)
278.2700	-33.2605	16.47 ± 7.62	26.39 ± 12.33	55.53 ± 4.91	N44L, N44 (HII region, IC 2128)
278.5779	-33.1640	5.81 ± 4.36	21.27 ± 10.91	36.55 ± 0.78	N44L, N44 (HII region, IC 2128)
280.2325	-32.7985	4.93 ± 2.56	9.73 ± 5.31	15.91 ± 0.35	N139 (Emission nebula)
276.1045	-33.2577	76.17 ± 26.47	91.11 ± 34.81	60.66 ± 4.69	N48B (NGC 1945)
276.0920	-33.2551	449.14 ± 194.29	163.66 ± 37.50	69.36 ± 7.86	N48B (NGC 1945)
276.1019	-33.2417	39.46 ± 13.10	619.49 ± 327.36	80.14 ± 7.53	N49 (SNR, HD 271255)
277.7323	-33.0396	9.56 ± 4.45	21.56 ± 5.84	41.78 ± 1.50	N51D (C1 object, NGC 1974)
277.8186	-32.9824	31.62 ± 8.17	60.14 ± 12.47	58.22 ± 2.05	N51D (C1 object, NGC 1974)
277.8173	-32.9749	19.18 ± 9.46	32.42 ± 13.82	53.08 ± 4.64	N51D (C1 object, NGC 1974)
277.4350	-32.8499	8.79 ± 3.51	11.09 ± 5.20	13.47 ± 0.56	S36 (Wolf-Rayet star), N51
275.4692	-33.0361	8.19 ± 3.39	28.84 ± 5.69	4.41 ± 0.08	
280.4771	-32.2126	3.83 ± 1.56	6.44 ± 3.68	27.44 ± 0.62	S117 (Blue Supergiant), N135
280.4365	-32.1865	4.81 ± 2.46	8.53 ± 3.74	20.28 ± 0.59	S117, N135 (NGC 2052)
280.4831	-31.9756	7.63 ± 3.52	13.96 ± 4.23	34.50 ± 0.71	N154B, N152 (C1 object, NGC 2033)
279.6733	-31.9713	102.20 ± 38.83	250.91 ± 70.544	146.32 ± 14.71	N154, N154B (C1 object, NGC 2033)
279.7307	-31.9578	12.12 ± 5.82	13.08 ± 6.42	60.25 ± 4.31	N154, N154B(C1 object, NGC 2033)
279.6334	-31.9436	278.78 ± 63.10	621.32 ± 125.29	369.12 ± 59.09	N154, N154B (C1 object, NGC 2033)
279.6684	-31.9397	86.03 ± 23.51	210.22 ± 32.28	162.81 ± 11.81	N154, N154B (C1 object, NGC 2033)
279.7035	-31.9358	95.93 ± 15.11	158.55 ± 28.12	86.95 ± 7.99	N154, N154B (C1 object, NGC 2033)
279.6674	-31.9327	101.77 ± 21.59	245.51 ± 45.39	187.02 ± 29.56	N154, N154B (C1 object, NGC 2033)
279.4482	-31.7298	585.03 ± 232.79	2337.53 ± 767.45	586.16 ± 81.12	N157A, N157A (HII region, HD 38268)
280.1003	-30.8812	9.15 ± 4.41	7.79 ± 3.67	54.74 ± 2.01	N170 (Emission nebula)
280.0631	-30.8595	27.85 ± 7.63	32.92 ± 8.59	55.09 ± 1.98	N170 (Emission nebula)
280.8937	-30.7529	7.99 ± 2.45	11.69 ± 5.57	19.43 ± 0.51	

Table 3.3: Rank correlation coefficients (ρ) for all '15' locations observed by *Spitzer* and separately for the '6' N11 locations.

Wavelength	ρ	p-value
8 μm vs. FUV 1A1	0.764	0.001
24 μm vs. FUV 1A1	0.314	0.254
8 μm vs. FUV 1A1 (N11)	0.828	0.041
24 μm vs. FUV 1A1 (N11)	0.885	0.018

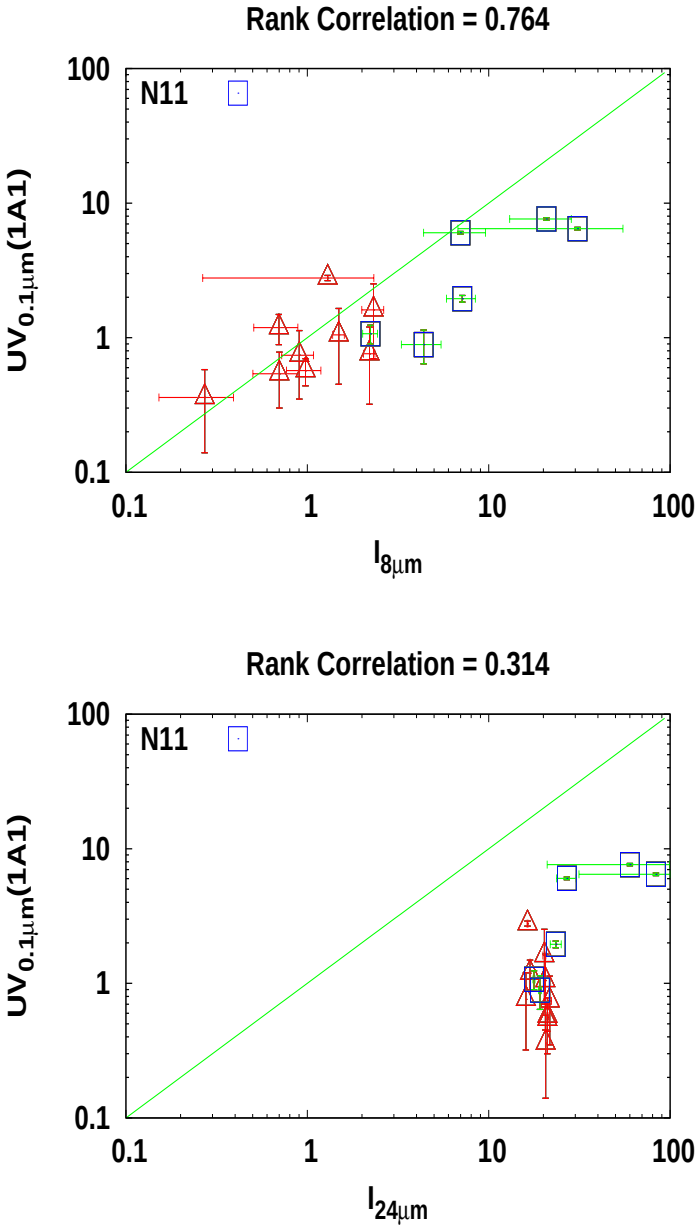

Figure 3.2: Correlations plotted for all 15 locations observed by *Spitzer* in the Large Magellanic Cloud.

Table 3.4: Rank correlation coefficients (ρ) for all '28' locations observed by *AKARI* and separately for the '8' 30 Doradus (30D) locations.

Wavelength	ρ	p-value
15 μm vs. FUV 1A1	0.493	0.007
24 μm vs. FUV 1A1	0.561	0.001
90 μm vs. FUV 1A1	0.644	0.001
15 μm vs. FUV 1A1 (30D)	0.514	0.191
24 μm vs. FUV 1A1 (30D)	0.431	0.286
90 μm vs. FUV 1A1 (30D)	0.419	0.301

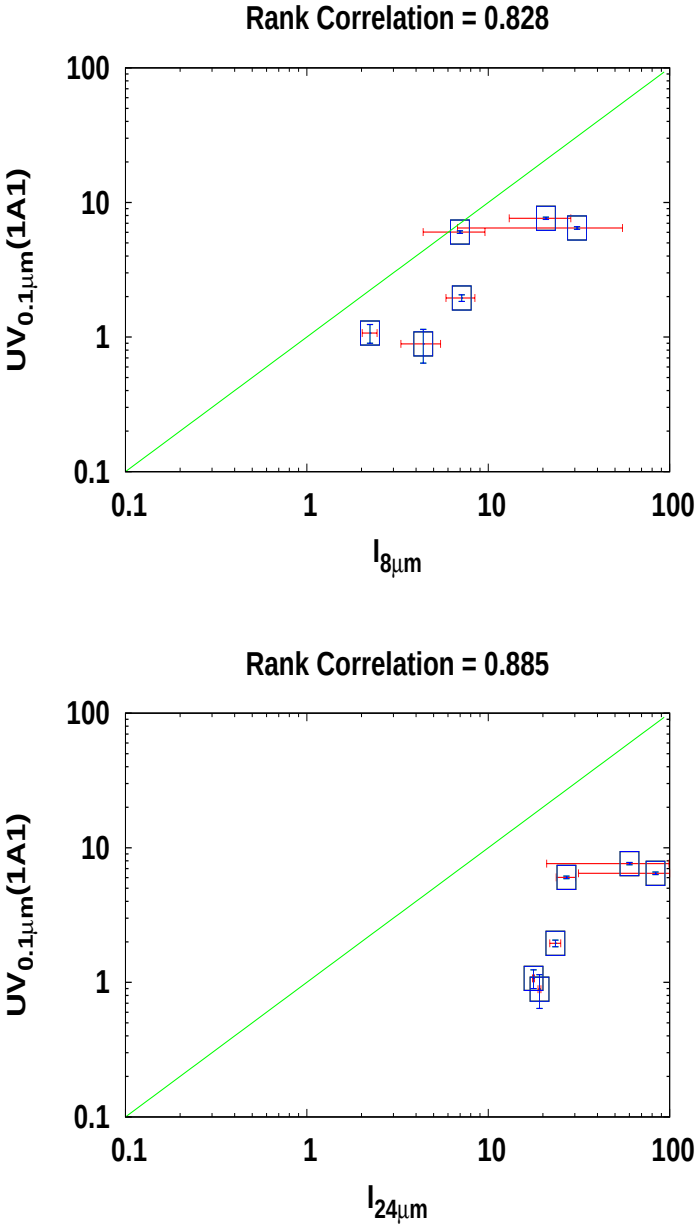

Figure 3.3: Correlations plotted for the 6 locations in the N11 region of the Large Magellanic Cloud observed by *Spitzer*.

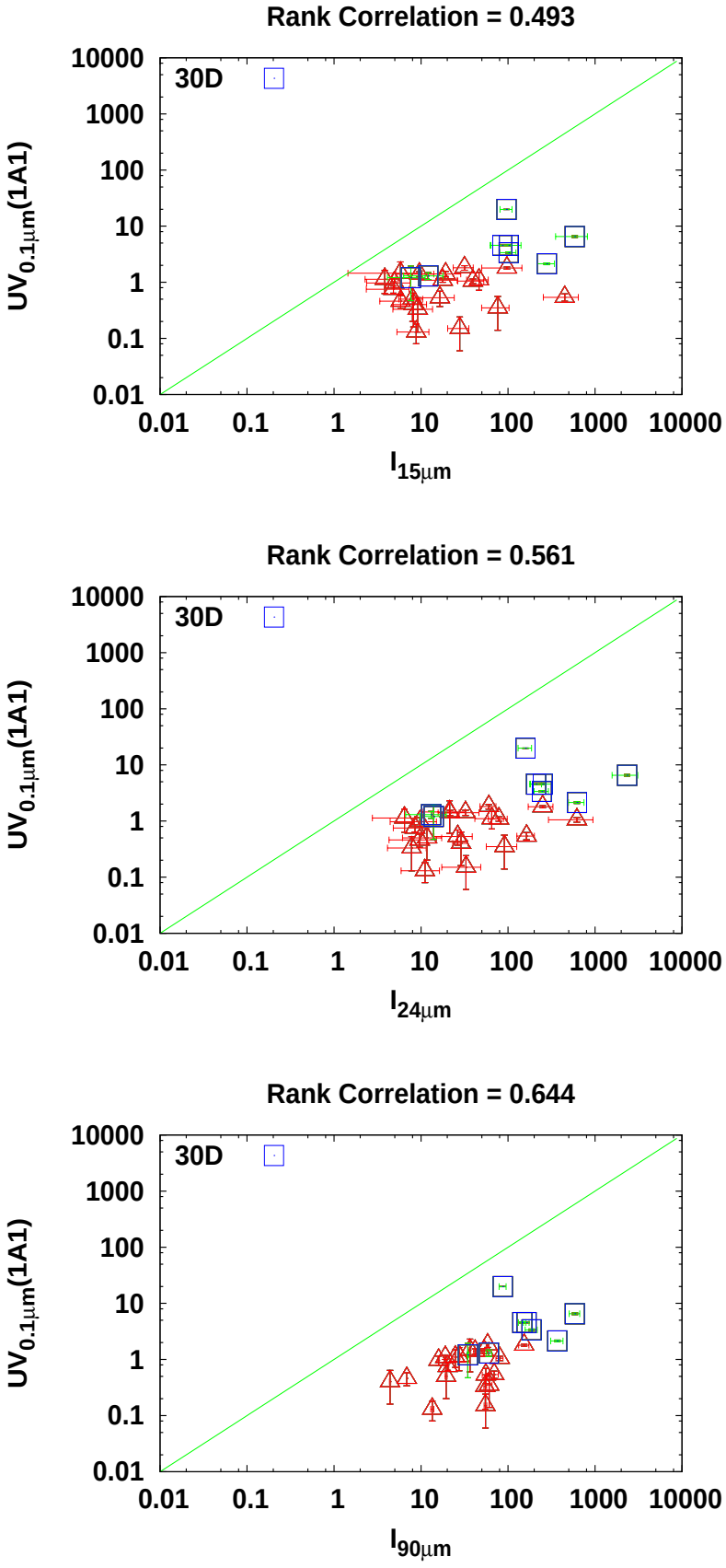

Figure 3.4: Correlations plotted for all 28 locations observed by *AKARI* in the Large Magellanic Cloud.

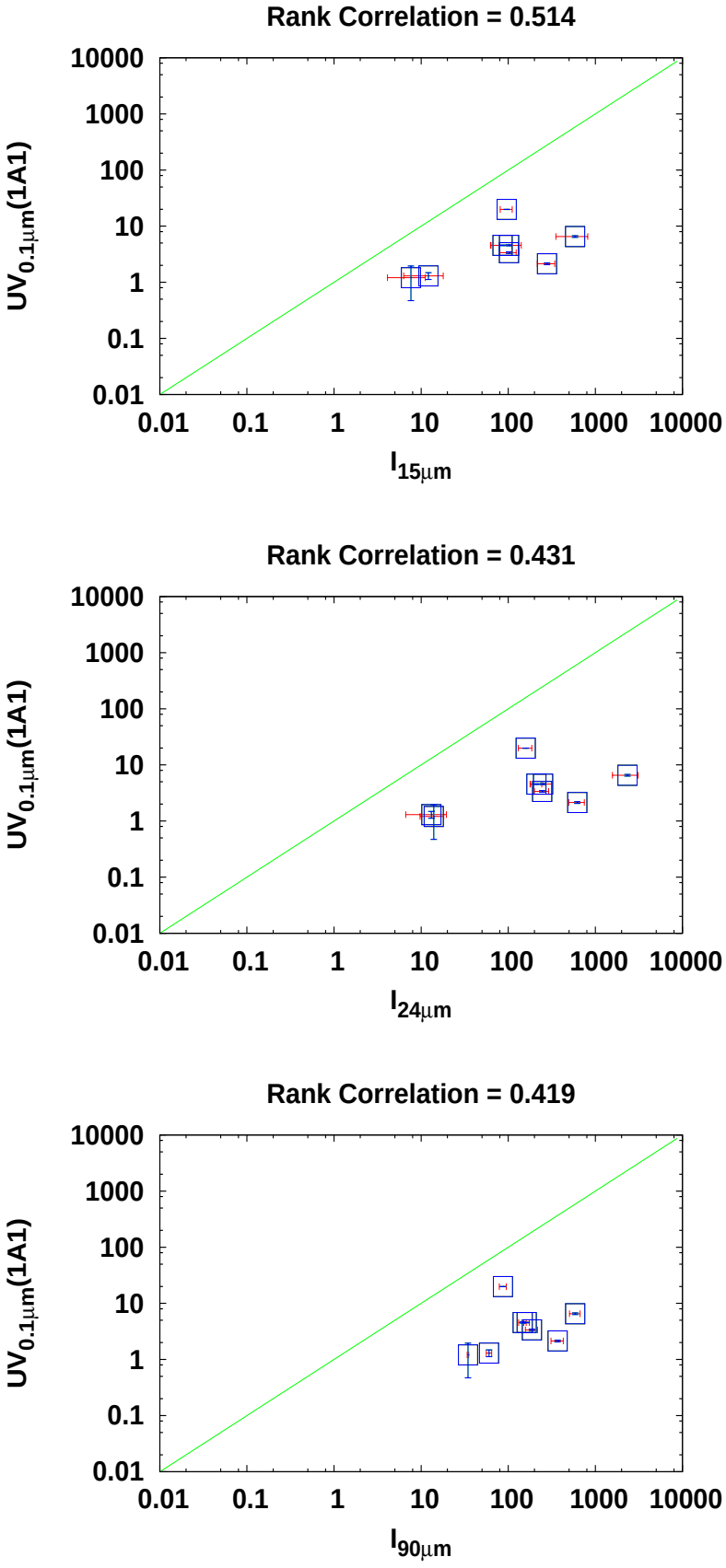

Figure 3.5: Correlations plotted for the 8 locations in the 30D region of the Large Magellanic Cloud observed by *AKARI*.

3.4 Discussion and Conclusions

The PAH mass fraction increases significantly towards molecular clouds except when there is a very strong radiation field since PAHs are likely to be destroyed in such a field [121]. The PAH mass fraction increases as one leaves the central OB stellar association. On the other hand, the VSG mass fraction increases at locations of an enhanced radiation field. Expanding bubbles may be launching dust at velocities that can cause big grains to shatter into VSGs causing 24 μm emission [121]. From Table 3.3 it is seen that when all 15 diffuse dust locations are taken together, the emission at 8 μm is much better correlated to the FUV intensity as compared to the emission at 24 μm, contrary to our initial assumptions. The FUV vs. 24 μm intensity correlation coefficient is not reliable due to the high p-value involved. This may be because these 15 locations contain a mixture of both hot and relatively cold regions of the LMC. Hot regions refer to the HII regions while cold regions refer to the general diffuse ISM. This is supported by the fact that we get a different correlation trend once we separate the N11 HII region from the other locations. In this case, we see that the FUV vs. 24 μm emission is marginally better correlated as compared to the FUV vs. 8 μm emission (Table 3.3). This supports the existing theory that the 24 μm VSG emission is seen to be associated with locations close to hot UV emitting stars present in HII regions, same as the dust scattered UV radiation. The high correlation value of FUV vs. 8 μm emission could possibly be attributed to the shielding of PAHs from destruction due to high-metallicity found in the LMC even in the vicinity of star-forming regions.

The 24 μm emission is known to be dominated by warm populations of VSGs which are mainly heated by young, massive stars. Results from *Spitzer* observations [104, 131, 132] have shown that the 24 μm luminosity is one of the best Star Formation Rate (SFR) indicators. *IRAS* and *ISO* observations have proved that the far-IR luminosity is also a good SFR tracer because of the emission peak around 65 μm due to dust heated by star formation. Thus, the 70 μm emission must be closely related to star formation activities and should have a tight and linear correlation with 24 μm warm dust emission [133]. We have found a very good correlation ($\sim$0.9) among the three *AKARI* wavelength bands: 15 μm, 24 μm and 90 μm, which shows that they are associated with VSGs from similar hot environments. This becomes more prominent when we take into consideration the 30 Doradus HII region. However, the FUV vs. IR correlations in the 30 Doradus HII region are not reliable due to the

high p-values associated with the coefficients. Hence, the 15 μm, 24 μm and 90 μm correlations with FUV are better when we consider all 28 *AKARI* locations as compared to when we consider only 30 Doradus. The FUV/IR(90 μm) ratio is a measure of the optical depth of the medium. We see that the average FUV/IR(90 μm) value in 30 Doradus is $\approx$0.0475 as compared to the lower average FUV/IR(90 μm) value in N11 at $\approx$0.01437. Hence, the lower correlation values in the 30 Doradus region may be attributed to it's higher FUV/IR(90 μm) ratio.

In conclusion, we have compared the diffuse dust emission in two HII regions of the LMC, namely N11 and 30 Doradus, and we observe better FUV vs. IR correlations for N11 ($\sim$0.8) as compared to the lower correlations ($\sim$0.5) with high p-values for 30 Doradus. We also observe a higher FUV/IR(90 μm) ratio for 30 Doradus in comparison to N11, which may indicate low extinction and/or much of the starlight being unaffected by interstellar dust. 30 Doradus is a very complex region with a high density of stars and therefore more starlight, as FUV can be contributed by unresolved stars. There is also a possibility of destruction of VSGs by highly energetic radiation in 30 Doradus leading to lower emissions around the 24 μm band. We hope to use the stellar/diffuse fraction which was presented by Pradhan et al. (2010) [130] and determine whether the stellar component of the FUV is indeed higher in 30 Doradus which has led to the observed correlation trends.